Inorg. Chem. **2003**, *42*, 2185–2187

Models for the Lower S States of Photosystem II: A Trinuclear Mixed-Valent $Mn^{II}/Mn^{IV}/Mn^{II}$ Complex

Maria Alexiou,[†] Catherine Dendrinou-Samara,[†] Anastasia Karagianni,[†] Subhashis Biswas,[‡] Curtis M. Zaleski,[‡] Jeff Kampf,[‡] Derek Yoder,[‡] James E. Penner-Hahn,[‡] Vincent L. Pecoraro,*[,‡] and Dimitris P. Kessissoglou*[,†]

Departments of Chemistry, Aristotle University of Thessaloniki, Thessaloniki, 54124, Greece, and University of Michigan, Ann Arbor, Michigan 48109-1055

Received September 20, 2002

The trinuclear complex $Mn_3(pko)_4(CH_3O)_2(SCN)_2 \cdot CH_3OH$, **1**, where Hpko is 2,2′-dipyridylketonoxime, is a rare example of a complex simultaneously containing Mn^{II} and Mn^{IV}. X-ray crystallography and XANES spectroscopy clearly distinguish the $Mn^{II}_2Mn^{IV}$ valence isomer from the more commonly observed $Mn^{III}_2Mn^{II}$ formulation. Fits to variable-temperature magnetic susceptibility data indicate that the Mn^{II} and Mn^{IV} are ferromagnetically coupled ($J = +6.13$ cm^{-1}) and that **1** has an $S = {}^{13}/_2$ ground state.

The photosynthetic conversion of water to dioxygen occurs in the oxygen evolving complex (OEC) of photosystem II. Four manganese ions form the heart of the water oxidation machinery of this enzyme.[1,2] There are five resolvable enzyme oxidation levels, termed S states, with the most reduced form being the S_0 level and the liberation of dioxygen occurring on the $S_3 \rightarrow S_4 \rightarrow S_0$ transition.[3] Numerous techniques have been used to probe the structure and oxidation states of the manganese ions in different S states. Originally X-ray absorption spectroscopy[4] and, more recently, EPR spectroscopy[5,6] have interrogated the S_0 oxidation level. On the basis of these studies, an ensemble of $Mn^{II}Mn^{III}Mn^{IV}_2$ has been proposed as the oxidation states for the S_0 manganese cluster.[4]

While low-nuclearity, mixed-valence manganese complexes are widely known, there are only two examples in which Mn^{II} coexists in the presence of Mn^{IV}. In most cases, the Mn^{II} and Mn^{IV} oxidation states are unstable to comproportionation reactions that yield Mn^{III}. Chan and Armstrong[7] reported a tetranuclear cluster of composition $Mn^{II}_2Mn^{III}$-Mn^{IV}. This molecule contained a $Mn^{III}Mn^{IV}$ μ-O core with peripheral Mn^{II} ions. Very recently,[8] one of us demonstrated that Mn^{II} and Mn^{IV} could exist in a tetranuclear cluster in the absence of Mn^{III}.

In this report, we present the first trinuclear manganese complex that contains only Mn^{II} and Mn^{IV} ions. Because of the linear topology of $Mn^{II}Mn^{IV}Mn^{II}(pko)_4(CH_3O)_2(SCN)_2 \cdot CH_3OH$, **1** [Hpko = 2,2′-dipyridyl ketonoxime], the magnetic interactions are more straightforward to analyze and this molecule is used to test whether XANES spectroscopy can distinguish a $[Mn^{II}_2Mn^{IV}]^{8+}$ species from $[Mn^{III}_2Mn^{II}]^{8+}$.

Complex **1** can be prepared by the addition of 1.2 mmol (0.24 g) of Hpko to a solution of 1.2 mmol (0.048 g) of sodium hydroxide and 0.6 mmol (0.081 g) of NaSCN in 50 mL of CH_3OH followed by 0.9 mmol (0.180 g) of $MnCl_2 \cdot 4H_2O$ dissolved in 50 mL of methanol. Then, the solution was exposed to dioxygen by bubbling air into the reaction mixture. The resulting black-red solution was reduced to 50 mL and then 10 mL of CH_2Cl_2 was added. Black-brown crystals suitable for X-ray diffraction studies were obtained by slow evaporation.[9] The Cl^- analogue is prepared analogously, omitting the NaSCN. On the basis of X-ray analysis, **1** and the Cl^- analogue are isostructral.

The neutral complex **1** (Figure 1) has 8 anions (2 thiocyanates, 2 μ-alkoxides, and 4 pko^- ligands) requiring that the sum of the charges on the 3 manganese ions be +8. We prefer the manganese oxidation state formulation of $[Mn^{II}_2Mn^{IV}]^{8+}$. The complex includes a central octahedral Mn(IV) ion, Mn(1) located on a crystallographic inversion center. It is flanked by two Mn(II) ions, Mn(2) and Mn-(2A). Each pko^- ligand acts as a tridentate chelating agent by using a pyridine, N(3), and an oximato nitrogen, N(1),

* Authors to whom correspondence should be addressed. E-mail: vlpec@umich.edu (V.L.P.); kessiog@chem.auth.gr (D.P.K.).
† Aristotle University of Thessaloniki.
‡ University of Michigan.

(1) Pecoraro, V. L.; Hsieh, W.-Y. In *Manganese and Its Role in Biological Processes*; Sigel, A., Sigel, H., Eds.; Marcel Dekker: New York, 2000; Vol. 37, p 429.
(2) Carrell, T. G.; Tyryshkin, A. M.; Dismukes, G. C. *J. Biol. Inorg. Chem.* **2002**, *7*, 2.
(3) Kok, B.; Forbush, B.; McGloid, M. *Photochem. Photobiol.* **1970**, *11*, 457.
(4) Yachandra, V. K.; Guiles, R. D.; McDermott, A.; Britt, R. D.; Cole, J.; Dexheimer, S. L.; Sauer, K.; Klein, M. P. *J. Phys., Colloq.* **1986**, No. C8, Vol. 2, 1121.
(5) Åhrling, K. A.; Peterson, S.; Styring, S. *Biochemistry* **1997**, *36*, 13148.
(6) Messinger, J.; Robblee, J. H.; Yu, W. O.; Sauer, K.; Yachandra, V. K.; Klein, M. P. *J. Am. Chem. Soc.* **1997**, *119*, 11349.
(7) Chan, M. K.; Armstrong, W. H. *J. Am. Chem. Soc.* **1990**, *112*, 4985.
(8) Afrati, T.; Dendrinou-Samara, C.; Raptopoulou, C. P.; Terzis, A.; Tangoulis, V.; Kessissoglou, D. P. *Angew. Chem., Int. Ed.* **2002**, *41*, 2148.

10.1021/ic026050h CCC: $25.00
Published on Web 03/06/2003

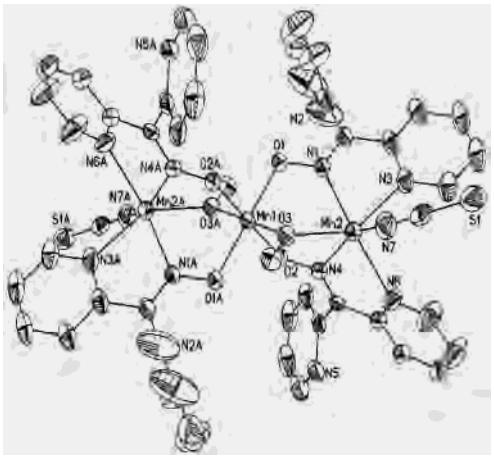

Figure 1. ORTEP diagram of **1**. Important bond lengths (Å) and angles (deg): $Mn(1)-O(1)_{oximato} = 1.922(2)$; $Mn(1)-O(2)_{oximato} = 1.933(2)$; $Mn(1)-O(3)_{methoxy} = 1.881(2)$; $Mn(2)-N(1)_{oximato} = 2.259(3)$; $Mn(2)-N(3)_{pyridyl} = 2.291(3)$; $Mn(2)-N(4)_{oximato} = 2.241(2)$; $Mn(2)-N(6)_{pyridyl} = 2.280(3)$; $Mn(2)-O(3)_{methoxy} = 2.150(2)$; $Mn(2)-N(7)_{thiocyanato} = 2.119(3)$; Mn(1)···Mn(2), 3.372; Mn(1)−O(3)−Mn(2), 113.39(10).

bound to Mn(II) ion and the oximato oxygen, O(1), coordinated to Mn(IV) central ion, while the other nitrogen atom of the pko ligand, N(2), remains uncoordinated. The terminal unidentate pseudohalide ligand is bound to Mn(II) ions through the nitrogen atom. The six bond distances around the Mn(1) atom average 1.91 Å varying from $Mn(1)-O(3)_{methoxy} = 1.881(2)$ Å to $Mn(1)-O(2)_{oximato} = 1.933(2)$ Å. The average distance is similar to those in mononuclear Mn(IV) compounds (e.g., $Mn^{IV}(SALADHP)_2$[11−13], $Mn-O_{av} = 1.889$ Å) and approximately 0.12 Å shorter than the average bond lengths that are typical for Mn^{III} species.

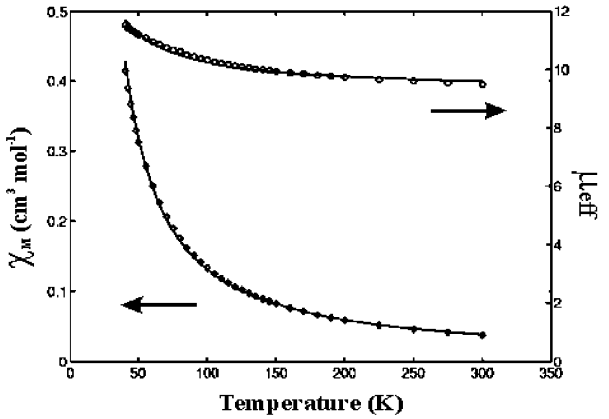

Figure 2. Variable-temperature magnetic susceptibility for **1**.

The lack of a Jahn−Teller distortion of Mn(1) further supports the oxidation state assignment as Mn^{IV} rather than Mn^{III}. The terminal Mn(2) ions are coordinated to five nitrogen atoms and an oxygen atom with an average bond distance of 2.223 Å (varying from 2.119(3) to 2.291(3) Å). This average value is typical for Mn(II) compounds and fully supports a valence trapped 2+ oxidation state for the terminal atoms. The central Mn(1) and the terminal Mn(2) ions, bridged by the methoxide oxygen and two oximato groups, are separated by 3.372 Å. It is interesting to compare the structure of **1** to previously reported trinuclear $Mn^{III}Mn^{II}$-Mn^{III} compounds, such as $Mn^{II}Mn^{III}_2(SALADHP)_2(OAc)_4(MeOH)_2$,[14,15] **2**, which also have an Mn_3^{8+} core. The Mn^{III} ion in this class of complexes has a $Mn-O_{av}$ distance of 2.031 Å with equatorial ligation averaging 1.926 Å and the axial distances being much longer (2.241 Å). The Mn^{II} ion is more symmetric and has an average distance of 2.154 Å. The average Mn···Mn separation is 3.486 Å. Thus, within the class of molecules containing a Mn_3^{8+} stoichiometry, **1** and **2** represent two distinct valence isomers.

The $Mn^{III}Mn^{II}Mn^{III}$ compounds showed weak antiferromagnetic exchange interactions ($J \sim -6$ cm^{-1}) with an $S = {}^3/_2$ ground state, whereas the tetranuclear $Mn^{II}_3Mn^{IV}$ exhibited both antiferromagnetic and ferromagnetic exchange. Therefore, we collected the variable-temperature magnetic susceptibility data[10] for **1**, shown as Figure 2, to discern the type of magnetic exchange interactions for this valence isomer. The best fit (for a model with J_{12} being defined as the exchange parameter between the central Mn^{IV} and terminal Mn^{II} and J_{22} set to 0) is $J_{12} = +6.13$ cm^{-1} and $g = 2.09$. The magnetic ground state, confirmed by magnetization measurements at 4.5 K, is $S = {}^{13}/_2$ (Figure S1, Supporting Information). Different EPR spectral signatures are found for **1** and **2** (Figure S2). **1** has unstructured, low field transitions at 4.2 K while **2** exhibits a broad feature, with multiline character centered around 1600 G.[14] Detailed interpretation of the EPR spectra is complicated by the large density of states for this complex (Figure S3, Supporting Information).

(9) Characterization of **1**. Elemental analysis with the formula $C_{49}H_{42}Mn_3N_{14}O_7S_2$ (fw = 1167.9) $Mn^{II}Mn^{IV}Mn^{II}(pko)_4(CH_3O)_2(SCN)_2\cdot CH_3OH$]. Yield: 65%. Anal. Calcd. C, 50.34; H, 3.59; N, 16.78; S, 5.47; Mn, 15.12. Found: C, 50.00; H, 3.55; N, 16.35; S, 5.47; Mn, 14.70. FAB-MS(+) (dmf solution) gives molecular ion $[Mn^{II}Mn^{IV}Mn^{II}(pko)_4(CH_3O)_2(SCN)_2]$. A crystal of dimensions 0.60 × 0.40 × 0.34 mm of **1** was analyzed. The integration of the data yielded a total of 16328 reflections to a maximum 2θ value of 53.20° of which 6404 were independent and 4504 were greater than $2\sigma(I)$. The final cell constants are ($a = 10.5410(8)$ Å; $b = 12.6576(10)$ Å; $c = 13.5251(10)$ Å; $\alpha = 80.010(3)°$; $\gamma = 70.670(3)°$. The structure was solved and refined using the space group $P\bar{1}$ with $Z = 1$ for the formula $C_{48}H_{38}N_{14}O_6S_2Mn_3\cdot(CH_3OH)$. All non-hydrogen atoms were refined anisotropically with the hydrogen placed in idealized positions. Full-matrix least-squares refinement based on F^2 converged at R1 = 0.0482 and wR2 = 0.1331 [based on $I > 2\sigma(I)$], R1 = 0.0747 and wR2 = 0.1436 for all data. Cyanate and chloride adducts, replacing thiocyanate, are isostructural with **1**.

(10) Variable-temperature DC SQUID measurements were collected on a Quantum Design MPMS Controller SQUID susceptometer (model 1822) equipped with a 5 T superconducting magnet over the range 5−300 K at a field of 5000 G. Powdered samples were used for data collection. Pascal's constants were used to determine the diamagnetic correction factors (Boudreaux, E. A.; Mulay, L. N. In *Theory & Applications of Molecular Paramagnetism*; John Wiley & Sons: New York, 1976; p 494. Drago, R. S. In *Physical Methods For Chemists*, 2nd ed.; Surfside Scientific Publishers: Gainesville, FL, 1992; p 471). The magnetic data were fit with the Van Vleck formula over the range 40−300 K. It was assumed that there was no interaction between the two Mn(II) centers. The *g* for Mn(II) was fixed at 2.0, and the *g* value for Mn(IV) was allowed to vary. The Van Vleck formula can be found in the Supporting Information.

(11) Li, X.; Lah, M. S.; Pecoraro, V. L. *Acta Crystallogr.* **1989**, *C45*, 1517.
(12) Kessissoglou, D. P.; Butler, W. M.; Pecoraro, V. L. *J. Chem. Soc., Chem. Commun.* **1986**, 1253.
(13) Kessissoglou, D. P.; Li, X.; Butler, W. M.; Pecoraro, V. L. *Inorg. Chem.* **1987**, *26*, 2487.
(14) Li, X.; Kessissoglou, D. P.; Kirk, M. L.; Pecoraro, V. L.; Bender, C. J. *Inorg. Chem.* **1988**, *27*, 1.
(15) Kessissoglou, D. P.; Kirk, M. L.; Bender, C. A.; Lah, M. S.; Pecoraro, V. L. *J. Chem. Soc., Chem. Commun.* **1989**, 84.

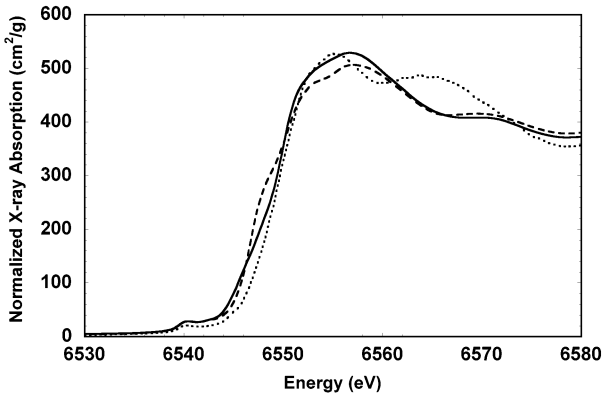

Figure 3. XANES spectra of **1** and **2** (**1** solid line, Cl^- analogue dashed line, **2** dotted line). The edge for **2** is narrower, starting at higher energy but maximizing at the same energy.

X-ray absorption spectra[16] for **1** and for the Cl^- analogue were nearly identical, with the biggest difference being a slightly broader Fourier transform for the Cl^- analogue (Figure S5, Supporting Information). Fits to the EXAFS[17] (Figure S5, S6, Table S1, Supporting Information) required two shells of nearest neighbors, at ca. 1.9 and 2.2 Å, as expected from the crystal structure. Fits for the two compounds are nearly identical, and, in particular, addition of 0.67 Mn−Cl per Mn did *not* significantly improve the fit for the Cl^- complex, despite the fact that Cl^- is unambiguously ligated to the Mn(II). For each complex, the Fourier transform shows two large peaks due to outer-shell scattering. These could be modeled using three shells of C/N scattering, giving distances consistent with the crystal structure of **1**. Due to the limited data range and the relatively large number of variable parameters, the coordination numbers for the C/N shells were constrained to match the crystallographic values. Despite the limited data range, the best-fit Mn−C/N distances were a good match to the crystallographic values. Inclusion of a Mn−Mn shell at 3.37 Å **(1)** or 3.41 Å (Cl^- complex) gave a small but reproducible improvement in the fit.

The XANES spectra were fit with linear combinations of Mn model spectra.[18,19] In both **1** and the Cl^- analogue, the best fit gave an average oxidation state of 2.7, consistent both with the $Mn^{II}_2Mn^{IV}$ assignment and with the $Mn^{III}_2Mn^{II}$ alternative. However, as shown in Figure 3, the XANES spectrum for an authentic $Mn^{III}_2Mn^{II}$ trimer, **2**, is somewhat narrower than that seen for **1** or for its Cl^- analogue (identical spectra are found for analogues of **2**), and has a weaker 1s−3d transition (Figure S6). Interestingly, there is no shift in 1s−3d energy (<0.2 eV), in contrast with the 2 eV shift observed between Cu^{II} and Cu^{III}.[20] This difference in XANES shape suggests that it may be possible to distinguish experimentally between the two valence configurations. When the XANES spectra for **1** were fit with a linear combination of Mn(II), Mn(III), and Mn(IV), the best fits all had less than 15% Mn(III), while the corresponding fits for **2** never gave more than 15% Mn(IV), consistent in both cases with the proposed oxidation state assignments. Similarly, fits of **1** using a linear combination of Mn(II) and Mn(IV) models were ca. 50% better than fits using a linear combination of Mn(II) and Mn(III). Comparable behavior was seen for **2**, where fits using Mn(II) + Mn(III) were ca. 70% better. These results suggest that, at least in some cases, it is possible to define not only the average oxidation state but also the distribution of oxidation states using XANES. Although the estimated accuracy for overall oxidation state determination is relatively poor (2.7 ± 0.2 for average oxidation state), there is nevertheless a clear difference in the quality of the fits when the correct oxidation state mixture is used. This, when combined with techniques such as EPR that can distinguish between even and odd numbers of unpaired electrons, is sufficient to define the oxidation state of complex multinuclear aggregates such as found in OEC.

Understanding the oxidation states and structure of S_0 in the OEC is second in importance only to defining the chemistry of the S_4 state that is responsible for water oxidation. This is because S_0 is the product state of the cycle. Using XANES spectroscopy, Klein et al.[21] made the assignment of the S_0 oxidation level as $Mn^{II}Mn^{III}Mn^{IV}_2$. We felt that it was important to prepare complexes that contained both Mn^{II} and Mn^{IV} in order to assess whether XANES could properly assign oxidation states for a complex containing a Mn^{II}, Mn^{IV} environment. Our XANES data show that an accurate oxidation assignment of the $Mn^{II}Mn^{IV}Mn^{II}$ cluster can be obtained and that Mn^{III} can clearly be eliminated as a reasonable formulation. We infer from this work that XANES should be able to discriminate the $Mn^{II}Mn^{III}Mn^{IV}_2$ composition for the OEC.

Acknowledgment. The authors thank the following agencies for support: V.L.P. (NIH GM39406), J.E.P.-H. (GM45205), D.P.K. (WG010 of COST action D21). The authors also thank Tsu-Chien Weng for help in fitting the magnetic data and preparing figures.

Supporting Information Available: The Van Vleck formula used for fitting magnetic data, Figure S1 (magnetic data for **1**), Figure S2 (EPR spectra of **1** and **2** at 4.2 K), Figure S3 (EPR spectrum of **1** at 4.2 K), Figure S4 (VT EPR of **1**), Figure S5 (FT data and best fits for **1** and the Cl^- analogue), Figure S6 and Table S1 (EXAFS and best fits of **1** and the Cl^- analogue), Figure S7 (expansion of 1s−3d region), Table S2 (XANES fit details), and X-ray crystallographic tables (PDF). This material is available free of charge via the Internet at http://pubs.acs.org.

IC026050H

(16) Measured at 10 K in transmission mode on SSRL line 7-3 using BN diluted powders, Si (220) double crystal monochromator detuned 50%. Energies calibrated by defining the preedge peak of $KMnO_4$, as 6543.3 eV.

(17) EXAFS were analyzed from $k = 2$ to 11.5 $Å^{-1}$ using AUTOBK and fit using IFFEFFIT (Newville, M. *J. Synchrotron Radiat.* **2001**, *8*, 322−324) with phase and amplitude functions from FEFF 7.02 (Ankudinov, A.; Ravel, B.; Rehr, J. J.; Conradson, S. *Phys. Rev. B* **1998**, *58*, 7565−7576).

(18) Riggs-Gelasco, P. J.; Mei, R.; Yocum, C. F.; Penner-Hahn, J. E. *J. Am. Chem. Soc.* **1996**, *118*, 2387.

(19) Fits were performed for all possible binary and ternary combinations drawn from a library of 8 Mn^{II}, 9 Mn^{III}, and 7 Mn^{IV} complexes. Uncertainty in oxidation state composition, based on the observed range of fit values, is approximately 10%.

(20) DuBois, J. L.; Mukherjee, P.; Stack, T. D. P.; Hedman, B.; Solomon, E. I.; Hodgson, K. O. *J. Am. Chem. Soc.* **2000**, *122*, 5775

(21) Roelofs, T. A.; Liang, W.; Latimer, M. J.; Cinco, R. M.; Rompel, A.; Andrews, J. C.; Sauer, K.; Yachandra, V. K.; Klein, M. P. *Proc. Natl. Acad. Sci. U.S.A.* **1996**, *93*, 3335.